Surface-Enhanced Raman Scattering from small numbers of purified and oxidised single-walled carbon nanotubes: Evidence for Stone-Thrower-Wales defects or amorphous carbon impurities.

Nebras Al-Alttar [1], Ilona Kopf [2], Eamonn Kennedy[1], Kevin Flavin[2], Silvia Giordani[2], James H Rice[1]

[1] School of Physics, University College Dublin, Belfield, Dublin 4, Ireland
[2] School of Chemistry/CRANN, Trinity College Dublin, Dublin 2, Ireland

Abstract

Surface enhanced resonance Raman scattering (SERRS) has been applied to investigate defects in purified and carboxylated single-walled carbon nanotubes (SWCNTs). For both samples SERRS spectra with temporal fluctuating peak intensities and positions in the range of 1000 to 1350 cm^{-1} have been observed. A series of peaks in this window were observed to coincide with peak positions that have been assigned to arise from Stone-Thrower-Wales and heptagonal-pentagonal intramolecular junction defects on the nanotubes surface. Two possible origins for these fluctuating spectral features are discussed ie the presence of Stone-Thrower-Wales defects in SWCNTs or amorphous carbon impurities.

1. Introduction

Single-walled carbon nanotubes (SWCNT) possess remarkable electrical, optical, thermal, and mechanic properties which make them attractive candidates for a variety of applications, ranging from material to life sciences. However, the inadequate purity, solubility, and processability of as-prepared SWCNTs impede their implementation in many applications. Furthermore the presence of contaminants renders it difficult to investigate and understand intrinsic physical and chemical properties of SWCNTs. Purification [1-5] and functionalization [6-9] strategies help to overcome these obstacles. However, a critical aspect that needs to be considered with regard to purification and functionalization strategies is the introduction of defect sites on the SWCNT surfaces. Defects play a significant role in nanomaterials as they affect the materials properties and can result in the loss of mechanical strength, change in optical activity and increase in electrical resistance. But defects are not necessarily negative. They can also result in interesting changes in properties producing exciting effects that lead to new applications. As example tailoring and covalent functionalisation of SWCNTs requires a certain density of defects as functional groups are attached to rehybridized defect sites (sp^2 to sp^3 rehybridized carbon atoms). Another example are topological defects such as pentagon-heptagon defect pairs which can introduce a change in chirality within the nanotube itself. Such defective SWCNTs can behave as nanoscale metal-semiconductor Schottky barriers [10] or nanodiodes [11] for nanoscale electronic devices. A precise understanding and control of defects in SWCNTs is required to exploit the opportunities they offer with regard to their applicability.

A versatile technique for the investigation of defects in SWCNTs is Raman spectroscopy. Raman spectra of SWCNTs show three important regions: i) the radial breathing mode (RBM) in the 150 to 350 cm^{-1} region, gives information on the diameter and chirality of SWCNTs, ii) the tangential mode (G-band), in the 1515 to 1590 cm^{-1} region displays distinctive behaviour modes for metallic and semiconducting SWCNTs, and iii) the disorder band (D-band) in the 1280 to 1320 cm^{-1} region arises from structural defects, amorphous

carbon, poor graphitization, and sp^3-hybridized (functionalized) carbons. Thus, by monitoring the Raman D band alterations in the hexagonal atomic structure can be investigated. Raman spectroscopy provides not only information on the defects but also a wealth of further information on SWCNTs. In surface enhanced Raman scattering (SERRS) the Raman signal of SWCNTs can be enhanced by up to 14 orders of magnitude [12-14]. This enables small numbers of nanotubes to be probed down to the single nanotube level [12, 13, 15]. SERRS can occur when the SWCNT is placed in contact with metallic (such as silver or gold) nanostructured materials [12, 13]. These nanomaterials enable enhancement via localised optical fields. The size of these localised regions can be on the order of 5 nm.

Raman and SERRS studies of SWCNTs have shown that defects such as topological defects can be observed. These kinds of defects refer to the presence of ring sizes other than hexagons, e.g. pentagons, hexagons, or octagons [16-18]. One such topological defect is adjacent pentagon/heptagon pairs, called Stone-Thrower-Wales (STW) and heptagonal-pentagonal intramolecular junction defects [16, 18]. As outlined by Miyamoto et al a STW defect consists of a localised $\pi/2$ rotation of a C-C bond, such that two pentagons and heptagons are created [19]. These pentagon and heptagon arrangements potentially translocate along the structure, creating either dislocation centres in regions of positive (pentagons) or negative (heptagons) Gaussian curvature, which ultimately lead to the closing of the nanostructure. Although the presence of STW defects changes the structural symmetry of the SWCNT and consequently vibrational modes associated with the topological defects are expected only a limited number of studies have been performed applying Raman spectroscopy to study these kind of defects on SWCNTs. Fujimori et al applied SERRS to detect STW defects in SWCNTs [16]. Temporally fluctuating spectra in SERRS occurred with additional peaks not observed in the non-SERRS spectra. These peaks were assigned to dynamic reconstruction of defective structures of SWCNTs arising from STW defects in the vicinity of SERRS-active sites under irradiation of the laser light.

SERRS studies of SWCNTs have also shown that studies using thin silver films (c.a. 10's nm) produces enhanced D band intensities and degradation of the SWCNT and the formation of particles similar to highly oriented pyrolytic graphite, C_{60} and amorphous carbon [20]. Lefrant et al reported that an interaction occurs between the nanotubes and the metal substrate creating conditions for degradation of SWCNTs, with metallic nanotubes primarily affected. Kudelski et al applied SERS to study carbon films deposited on roughed silver and gold surfaces [21]. The authors reported temporal fluctuations in the SERS features with distinct sets of intense and narrow Raman lines appear which were assigned to carbonaceous groups.

Here we perform a comparative SERRS studies on two kind of SWCNTs: i) commercial available purified SWCNTs and ii) highly purified and carboxylated SWCNTs with preserved optical/electronic properties [2]. In this study only purified SWCNTs have been used since they are free of metallic and carbonaceous impurities, whose Raman signals interfere with the SWCNT spectroscopic signature. SERRS spectra with randomly fluctuating peak intensities and positions in the 1000 to 1200 cm^{-1} frequency range have been observed. A series of peaks in this window coincides with peak positions that have been assigned to arise from defects on the nanotubes surface [16, 18]. We find that these peaks also occur for chemically treated SWCNTS. Our studies suggest that two possible assignments exist for these spectral features are presented ie the presence of Stone-Thrower-Wales defects or amorphous carbon impurities.

2. Experimental

SERRS measurements were carried out with a single monochromator (Roper Acton SP2300s) and EMCCD (Andor IXON) in a backscattering configuration using a 60× objective to excite and collect the scattered light. The spectral resolution was >1.5 cm^{-1} the power density on the sample was 0.65 MW cm^2. SERRS measurements were performed with 532 nm (Nd:YAG laser) and 632 nm excitation. The SERRS substrates consisted of c.a. 10 nm silver nanoparticles on top of a 40 nm thin film of silver which was deposited on a glass slide by vacuum deposition. SWCNTs were dispersed at low concentration in ethanol (abs) by sonication, spray coated onto freshly prepared SERRS substrates and dried in a desiccator. Purified commercially available SWCNTs (p-SWCNTs) were purchased from Carbon Nanotechnologies, Inc. and used as supplied. Highly purified and carboxylated SWCNTs (o-SWCNTs) were prepared according to a recently published purification/oxidation protocol [2]. Briefly, this method involves a short nitric acid oxidation to minimize structural/electronic degradation of SWCNTs and sodium hydroxide treatments to remove carboxylated carbonaceous impurities. A hydrogen peroxide oxidization step efficiently etches remaining carbonaceous impurities and ensures full oxidation of oxygenated species to carboxylic acid moieties. Persistence of characteristic optical properties indicating the preservation of the electronic structure during chemical treatment has been demonstrated [2]. Atomic Force Microscopy (AFM) images were recorded in dynamic mode using a NTEGRA Spectra (NT-MDT) with commercial available Si cantilever (NSG01, NT-MDT) as well as an explorer AFM system.

3. Results and discussion

SERRS of p-SWCNTs are shown in Fig. 1. Fig 1a presents intensity plots of SERRS spectra of p-SWCNTs recorded sequentially with a 10 s interval. The SERRS spectra show temporally fluctuating peaks superimposed on the G and D band regions. Areas of the sample that show the presence of these fluctuating peaks are found randomly across the sample with some regions of the sample showing no sharp fluctuating peaks, only broadened G and D bands with stable profiles. Fig 1b displays two SERRS spectra taken from different regions of the sample. One spectra show broadened G and D band features, the second spectrum shows sharp features within the G and D band region. The G and D modes are broadened compared to the Raman spectra. Broadening of the G and D band regions in SWCNT has been reported to occur for nanotubes on thin (c.a. >20 nm) silver films [20]. Fig 1c shows a sequence of ten spectra recorded over a concurrent period of time. Fluctuating peaks are seen in this spectral sequence with band positions and band intensities changing. Carbon nanotubes possess strong Raman scattering cross sections which when coupled with plasmonic enhancement enables small number of nanotubes to be observed down to the single nanotube level. The effect of ensemble averaging potentially gives rise to temporal fluctuations of intensities and frequencies. With SWCNTs of different sizes and orientations been observed at different times creating temporally fluctuating spectral signals.

In order to assess the type of nanotube probed a study of the radial breathing mode (RBM) region was undertaken. Fig 1d and e show RBM regions of SERRS spectra of p- and o-SWCNTs acquired with an excitation of 632 nm (Fig. 1d) and 532 nm (Fig. 1e). The RBM frequency of SWCNTs is inversely proportional to the tube diameter. Thus, the tube diameter can be calculated according to $\omega_{RBM} = 248/d_t$, where ω_{RBM} and d_t indicate the RBM frequency and tube diameter, respectively [12, 13]. Maultzsch et al applied resonant Raman to study the radial breathing mode of nanotubes for more than 50 chiral indices with

diameters between 0.6 and 1.5 nm [22]. The authors noted that $\omega_{RBM} = 248/d_t + C$ is required to more correctly account for additional external forces, e.g., from interactions with a substrate or neighbouring tubes in a bundle. The silver SERRS active potential creates additional external forces on the nanotube thus requiring correction for estimation of the ω_{RBM}, however it is noted that changes in the environment of the tubes probed so far lead to small changes in the RBM frequencies. To this end we did not take into account a correction factor but estimated the diameter according to $\omega_{RBM} = 248/d_t$. Using an excitation wavelength of 632 nm (Fig. 1d) RBM peaks at 283, 257 217 and 196 cm^{-1} corresponding to diameters of 1.14, 1.04, 0.88, 0.79 nm are found for p-SWCNTs while for o-SWCNTs peaks at 282, 255 218 and 198 cm^{-1} occur originating from nanotubes with a diameters of 1.14, 1.03, 0.88, 0.8 nm. Changing the excitation wavelength to 532 nm (Fig 1e), changes also the RBM spectrum as SWCNTs with different chiralities are excited. For p-SWCNTs peaks at 271, 240 and 192 cm^{-1} are observed meaning that tubes with a diameter d_t = 0.92, 1.03, and 1.29 nm are resonantly excited. O-SWCNTs possess peaks at 241 and 268 cm^{-1} which originate from nanotubes with d_t = 1.02 nm and 0.95 nm, respectively. According to the Kataura plot at an excitation wavelength of 532 nm (2.33 eV) RBM peaks between 200 and 275 cm^{-1} arise from metallic nanotubes and those above 275 cm^{-1} from semiconducting tubes [22]. At an excitation wavelength of 632 nm only RBM bands below 225 cm^{-1} belong to metallic nanotubes while the bands above 225 cm^{-1} arise from semiconducting nanotubes. With regard to the peak positions in our RBM SERRS spectra for p- and o-SWCNT this means that at 532 nm excitation predominantly metallic nanotubes are excited while predominantly semiconducting nanotubes are excited at 632 nm. These sizes of nanotube can be related tentatively to nanotube chirality. Kurti et al using density functional theory obtained the geometrical properties and the radial breathing mode (RBM) frequency of a series of 40 different single-walled carbon nanotubes [23]. The authors predicted that a (9,9) nanotube would have a RBM peak at 192 cm^{-1} and a (12,0) nanotube would have a RBM peak at 240 cm^{-1}. However it is noted for example that there the assignment of the chirality of the nanotube at the diameter 1.3 nm can be made to several nanotubes such as (9,9) and also to (10,m) were m = 7, 8 or 9. The broad RBM peaks potential possess a number of peaks corresponding to different nanotube chirality within this broad RBM envelop.

Studies of defects in nanotubes such as STW have been performed by Fujimori et al and Vandescuren et al [16, 18]. Fujimori et al reported temporally fluctuating SERRS spectra from SWCNTs with peaks in the D and G band regions and also peaks outside this region at 1139 and 1184 cm^{-1} which were assigned to dynamic reconstruction of defective structures of SWCNTs arising from STW defects in the vicinity of SERRS-active sites under irradiation of the laser light [16]. This study was based on semiconductor nanotubes with diameters of c.a. 1.5 and 1.3 nm. Theoretical calculations by Vandescuren et al predicted Raman peaks for STW defects for (10, m) (where m is an integer between 0 and 10) nanotubes and for heptagonal-pentagonal defects for (9,0) and (12,0) nanotubes [18]. The SERRS study here potentially probes both (10, m) and (12,0) nanotube type as evidenced by the RBM spectra (see above).

Fig 2 displays SERRS spectra, i to iii, selected from the spectra shown in Fig 2a. Spectra i and ii possess peaks at 1143 cm^{-1} as well as peaks at 1186 cm^{-1} both marked α. These bands are outside of the D and G wavelength region. The presence of the α bands is accompanied by a strong band in the G band region at c.a. 1590 cm^{-1}. Fig 2b shows that the bands marked α are persistent over seconds. Analysis of the spectral features in Fig 2a show the presence of a band at 1270 cm^{-1} (marked β). Spectrum iii in Fig 2a does not possess spectral features at α or β. Peaks (marked χ) are seen at 1276 and 1310 cm^{-1}.

The intensity of several peaks as a function of time was assessed by plotting band intensity vs. time over a 250 sec interval (as shown in Fig 2c). Inspection of Fig 2c shows that the bands at 1142 and 1186 cm^{-1} (assigned to STW defects) show similar fluctuations in Raman signal intensity with time. The band at 1270 cm^{-1} can also be assigned to arise from STW defects and shows a similar fluctuation in Raman signal intensity over time compared to the bands at 1142 and 1186 cm^{-1}. Looking at the Raman intensity over time for a band at 1599 cm^{-1}, which is associated with a SWCNT G mode, the intensity fluctuations visible differ to the bands associated with STW defects. Calculating the Pearson product-moment correlation coefficient r for the intensity allows for analysis of the 'randomnes' in the intensity of peaks [24]. Values close to zero indicate a random intensity variation while large values present a strong linear correlation. The Pearson product-moment correlation coefficient for the fluctuations in the α peak at 1183 cm^{-1} over the observed time-frame was as calculated to be $r = 0.27$. This indicates that the intensity variation is random over the recorded time window. Pearson product-moment correlation coefficient was employed to calculate the correlation between two Raman peaks by comparing the Raman signal intensities as a function of time i.e. when comparing two peaks. The variation of peak intensity of the two peaks at 1183 and 1142 cm^{-1} yields a correlation coefficient $r = 0.98$. This value demonstrates a strong correlation between the two Raman bands. Both bands are predicted to arise from STW defects. Another band that was predicted to be associated with STW defects is the band at 1270 cm^{-1}. Comparing the peaks at 1142 cm^{-1} with the band at 1270 cm^{-1} revealed a strong correlation $r = 0.94$. This supports the assertion that the peaks at 1270 cm^{-1} is associated with STW defects. A relatively minor correlations ($r = 0.47$ and 0.46 respectively) were found between the STW peaks at 1142 or 1183 cm^{-1} when compared to the peak at 1598 cm^{-1} which is associated with the G band in SWCNTs.

Fig 3 outlines the variation in Raman frequencies and intensities recorded for p-SWCNTs recorded at 632 nm. Fig 3a shows ten spectra recorded successively. Fig 3b shows the un-normalized spectra as shown in Fig 3a. The spectra show the presence of fluctuating peaks and a changing intensity in the spectral features. Magnifications of three spectra from Fig 3a are displayed in Fig 3c. The upper spectrum in Fig 3c shows peaks at 1144 and 1185 cm^{-1} (marked α). A band at 1269 cm^{-1} (marked β) is observed. These peaks are in the same position as the bands observed at 532 nm excitation. On this basis these peaks are assigned to dynamic reconstruction of defective structures of SWCNTs arising from STW defects in the vicinity of SERRS-active sites under irradiation of the laser light [16]. A small shift from 1139 to 1143 cm^{-1} or 1184 to 1186 cm^{-1} is present however. Theoretical calculations by Vandescuren et al predicted further Raman peaks for STW defects at 1270 and 1020 cm^{-1} [18]. The peak positions and intensities predicted by Vandescuren et al was for (10, m) SWCNT [18]. Analysis of the spectral features in Fig 2 and 3 show the presence of a band at 1270 cm^{-1} (marked β). While a band at 1020 cm^{-1} does not clearly appear. However, it is noted that the predicted band intensity at 1020 cm^{-1} is much weaker than the predicted band intensity at 1270 cm^{-1}. Spectra in Fig 2 and 3 also can show peaks (marked χ) at 1276 and 1310 cm^{-1}. These bands can be assigned, on the basis of theoretical calculations by Vandescuren et al, to heptagonal-pentagonal intramolecular junctions in carbon nanotubes, which correspond to defect modes localized on the pentagon and slightly around it [18]. These bands are reported to occur at 1275 and 1315 cm^{-1}.

Fig 4 outlines the variation in Raman frequencies and intensities recorded for o-SWCNTs recorded at 632 nm. Fig 4a shows ten spectra recorded successively. Fig 4b shows normalized spectra as shown in Fig 4a. The spectra show the presence of fluctuating peaks

and a changing intensity in the spectral features. The upper spectrum possesses peaks at 1143 cm^{-1} as well as peaks at 1186 cm^{-1} both marked α. Analysis of the spectral features shows also the presence of a band at 1270 cm^{-1} (marked β). The lower spectrum in Fig 4a does not possess spectral features at α or β. Peaks (marked χ) are seen at 1276 and 1310 cm^{-1}. These bands are in the same position and possess similar relative intensities are the bands marked correspondingly for p-SWCNT excited at 632 nm (as shown in Fig 3). This shows the treatment to produce the oxidised SWCNT (o-SWCNT) does not change the presence of bands potentially arising from defect sites.

Characterization of our SERS samples was carried out using AFM and optical microscopy. Optical microscopy revealed that the silver film deposited on the glass slides is not a continuous film but is fragmented into smaller and larger pieces on length scales of microns to millimetres. Fig 5c shows an AFM topography image of the surface features of the SERS substrate on which the SWCNTs are deposited. An inhomogeneous surface topography was found with surface roughness on the order of 10's to 100's of nm (Fig. 5b). The fragmentation of the silver film on the micro to mm scale in combination with the roughness created by the deposition of silver nanoparticles generates inhomogeneously distributed 'hot spot' areas with high plasmon enhancement. AFM studies on the SERS samples were performed to obtain in addition to the SERRS spectra information on the spatial distribution and aggregation state of the deposited SWCNTs. Although the surface is very rough it is possible to detect sometimes SWCNT bundles on the substrate (Fig. 5c inset). However, a conclusion on the distribution and aggregation state of the deposited SWCNTs is impossible on such a rough surface. To this end we replaced the SERS substrate by a cleaned smooth glass slide and deposited the SWCNTs in the same manner that we used for SERS sample preparation. AFM measurements on these samples revealed inhomogeneous distributed small bundles consisting only of a few nanotubes as well as individual SWCNTs (Fig.5d). The inhomogeneous distributions of plasmonic active silver 'hot spots' and SWCNTs explains the random occurrence of regions showing temporal fluctuating SERRS signals. Thus a variation in the SERS signal is especially expected when using a high power objective (ie 60X) which enables to probe small sample areas of only a few microns. Fluctuations in the SERRS Raman band intensities and positions have been observed previously and have been proposed to arise from the presence of such create plasmon enhancement "hot spots" on SERRS-active metals such as silver.

Molecular dynamic simulations were undertaken using MM+ methodology. The simulation was based on silver ions and a nanotube structure. The ions were calculated to interact with the nanotube. The ions were found to enter the nanotube and assemble with the nanotube and around its external structure, were the silver was placed at the beginning of the calculation. This simulation provides evidence that the silver ions are in proximity to the nanotube surface and as a consequence may interact with defect sites such as a mobile STW defect that may be present from a vacancy in the tube. The presence of these silver ions potentially influence the nanotubes structure and in turn the resulting Raman spectra. In addition it is noted that the presence of the nanoscale rough silver environment may lead to restricting the vibration motion of the nanotube leading to in turn a change in the frequency and intensity of the resulting Raman. The observed SERRS temporal Raman spectral features may result from a perturbation of the Raman modes and not by the presence of defects.

o-SWCNTs were prepared using a short acid/base treatment followed by a hydrogen peroxide oxidation ensuring full oxidation of oxygenated species to carboxylic acid groups. The presence of the carboxylic acid groups do not remove the occurrence of bands associated with

STW defects. The observed SERRS spectrum is modified compared to the Raman spectra for both the p-SWCNT and o-SWCNT as evidenced by the large D band SERRS intensity compared to the spectral features for the resonance Raman spectral features [2]. The intense D band in the SERRS indicates a change in the degree of disorder. The D band in the SERRS increases its intensity and displays a change in profile. The broadening of the D and G band region has been assigned to an interaction between the silver and the nanotube centring on the charge transfer mechanism responsible (in part) for the SERRS enhancement [20]. The presence of the silver nanoparticle layer potentially contributes also to this broadening and enhancement of the D band region.

Photo-induced structural changes such as the decomposition of the nanotube can potentially lead to the observation of bands in the c.a. 1150 cm^{-1} region assigned to STW defects as outlined above. Lefrant et al showed that SERRS from SWCNT could be interpreted in terms of degradation of the single-walled nanotubes and the formation of particles similar to highly oriented pyrolytic graphite e.g. C_{60} and amorphous carbon [20]. Lefrant et al demonstrated that the presence of materials such as C_{60} is expected to result in Raman spectra with marker bands at 1458 cm^{-1} [20]. No bands were observed at this position in the SERRS spectra indicating that the no C_{60} was formed. However the broad G and D bands seen in Fig 1b and 3a indicates that there is strong coupling between the SWCNT and the silver substrate. This coupling is expected to lead to strong SERRS. Studies by Kudelski [21] on the SERS of a carbon film assigned to amorphous carbon (bur potentially also containing pyrolytic graphite) was studied. Kudelski et al [21] assigned the SERS as arising from surface enhancement for species adsorbed at plasmon 'hot spots' on the metal surface with the spectral fluctuations indicating continuously progressing surface chemistry at discrete locations. The reported temporal Raman features in this study [21] resemble the spectral features reported here. Studies have shown that for o-SWCNT compounds are highly pure, with carbon based impurities been removed. However the creation of amorphous carbon and or pyrolytic graphite compounds via the interaction of the nanotubes with the metallic substrates in the absence or presence of the Raman excitation radiation (at with oxygen also present) potentially may occur. On this basis the contribution from amorphous carbon and or pyrolytic graphite compounds present as impurities in the sample or from degradation of the SWCNT cannot be ruled out.

4. Conclusion

SERRS studies on commercially available purified SWCNTs and highly purified and carboxylated SWCNTs have been carried out. For both samples SERRS spectra with and without temporal fluctuations in peak frequencies and intensities were found depending upon the area probed. The origin for the SERRS spectra with temporal fluctuations in peak frequencies and intensities was ascribed to single and/or few nanotubes been located in regions of the sample that possessed high plasmon localisation. Areas of relatively high and low plasmon localisation result from the rough surface topography of the silver substrate. In p-SWCNTs and o-SWCNT temporal fluctuating peaks in the region between 1000 to 1350 cm^{-1} Raman shift have been ascribed to the dynamic behaviour of STW and heptagonal-pentagonal intramolecular junction defects based on comparing the band positions observed to simulated values for the occurrence of such defects in nanotubes. Evidence for carbonaceous impurities photochemically generated in the sample was not definitively found, e.g. no occurrence of Raman bands at c.a. 1458 cm^{-1} (definitive for C_{60}) was observed when Raman bands for STW defects were observed. However contribution from amorphous carbon

and or pyrolytic graphite compounds present as impurities in the sample or from degradation of the SWCNT cannot be ruled out.

The treatment that creates the o-SWCNT nanotubes potentially can lead to a covalent bond occurring at a defect site. The occurrence of strong D band intensities indicates that potentially disorder/defects may be present on the nanotubes surface in o-SWCNTs as well as p-SWCNTs. MM+ calculations show that silver ions may be present within the tubes structure as well as near its external wall structure, these ions potentally perturbing the nanotubes structure and Raman spectral features. While the presence of photo-induced decomposition cannot be ruled out and also potentially impurities from the atmosphere or from contamination elsewhere may explain the observed bands, the occurrence of bands in the positions labelled α and β have been calculated to occur from defects in graphene.

Acknowledgment

The authors acknowledge Science Foundation Ireland (PIYRA 07/YI2/I1052 and TIDA Feasibility 10) for support. We acknowledge the support from the Iraq government for their postgraduate studentship for Nebras Al-Alttar. The authors are also grateful for the work of Alexei Kudryashov in data analysis.

References

1.Del Canto, E., et al., Critical Investigation of Defect Site Functionalization on Single-Walled Carbon Nanotubes. Chemistry of Materials, 2011. 23(1): p. 67-74.

2.Flavin, K., et al., Controlled carboxylic acid introduction: a route to highly purified oxidised single-walled carbon nanotubes. Journal of Materials Chemistry, 2011. 21(44).

3.Movia, D., E.D. Canto, and S. Giordani, Purified and Oxidized Single-Walled Carbon Nanotubes as Robust Near-IR Fluorescent Probes for Molecular Imaging. The Journal of Physical Chemistry C, 2010. 114(43): p. 18407-18413.

4.Movia, D., E. Del Canto, and S. Giordani, Spectroscopy of single-walled carbon nanotubes in aqueous surfactant dispersion. physica status solidi (b), 2009. 246(11-12): p. 2704-2707.

5.Park, T.-J., et al., Purification strategies and purity visualization techniques for single-walled carbon nanotubes. Journal of Materials Chemistry, 2006. 16(2).

6. Del Canto, E., et al., Functionalization of single-walled carbon nanotubes with optically switchable spiropyrans. Carbon, 2010. 48(10): p. 2815-2824.

7. Flavin, K., et al., Synthesis and Characterization of Boron Azadipyrromethene Single-Wall Carbon Nanotube Electron Donor−Acceptor Conjugates. ACS Nano, 2011.

8. Giordani, S., et al., Multifunctional hybrid materials composed of [60]fullerene-based functionalized-single-walled carbon nanotubes. Carbon, 2009. 47(3): p. 578-588.

9. Singh, P., et al., Organic functionalisation and characterisation of single-walled carbon nanotubes. Chemical Society Reviews, 2009. 38(8).

10. Louie, S., Electronic Properties, Junctions, and Defects of Carbon Nanotubes

11.Charlier, J.C., Defects in Carbon Nanotubes. Accounts of Chemical Research, 2002. 35(12): p. 1063-1069.

12. Kneipp, K., et al., Surface–enhanced Raman scattering on single–wall carbon nanotubes. Philosophical Transactions of the Royal Society of London. Series A: Mathematical, Physical and Engineering Sciences, 2004. 362(1824): p. 2361-2373.

13. Kneipp, K., et al., Coupling and scattering power exchange between phonon modes observed in surface-enhanced Raman spectra of single-wall carbon nanotubes on silver colloidal clusters. Physical Review B, 2001. 63(19): p. 193411.

14. Lordan, F., et al., Site selective surface enhanced Raman on nanostructured cavities. Applied Physics Letters, 2011. 99(3): p. 033104-3.

15. Zhang, Y., et al., Raman Spectra Variation of Partially Suspended Individual Single-Walled Carbon Nanotubes. The Journal of Physical Chemistry C, 2007. 111(5): p. 1983-1987.

16. Fujimori, T., et al., Evidence of Dynamic Pentagon−Heptagon Pairs in Single-Wall Carbon Nanotubes using Surface-Enhanced Raman Scattering. Journal of the American Chemical Society, 2010. 132(19): p. 6764-6767.

17. Stone, A.J. and D.J. Wales, Theoretical studies of icosahedral C60 and some related species. Chemical Physics Letters, 1986. 128(5–6): p. 501-503.

18. Vandescuren, M., et al., Characterization of single-walled carbon nanotubes containing defects from their local vibrational densities of states. Carbon, 2007. 45(2): p. 349-356.

19. Miyamoto, Y., et al., Spectroscopic characterization of Stone-Wales defects in nanotubes. Physical Review B, 2004. 69(12): p. 121413.

20. Lefrant, S., et al., Modification of surface-enhanced Raman scattering spectra of single-walled carbon nanotubes as a function of nanotube film thickness. Physical Review B, 2002. 65(23): p. 235401.

21. Kudelski, A, Pettinger, B, SERS on carbon chain segments: monitoring locally surface chemistry. Chemical Physics Letters, 2000, 321: p. 356–362

22. Maultzsch, J., et al., Radial breathing mode of single-walled carbon nanotubes: Optical transition energies and chiral-index assignment. Physical Review B, 2005. 72(20): p. 205438.

23. Kürti, J., et al., The geometry and the radial breathing mode of carbon nanotubes: beyond the ideal behaviour. New Journal of Physics, 2003. 5(1): p. 125.

24. Rice, J.H., et al., Temporal variation in photoluminescence from single InGaN quantum dots. Applied Physics Letters, 2004. 84(20): p. 4110-4112.

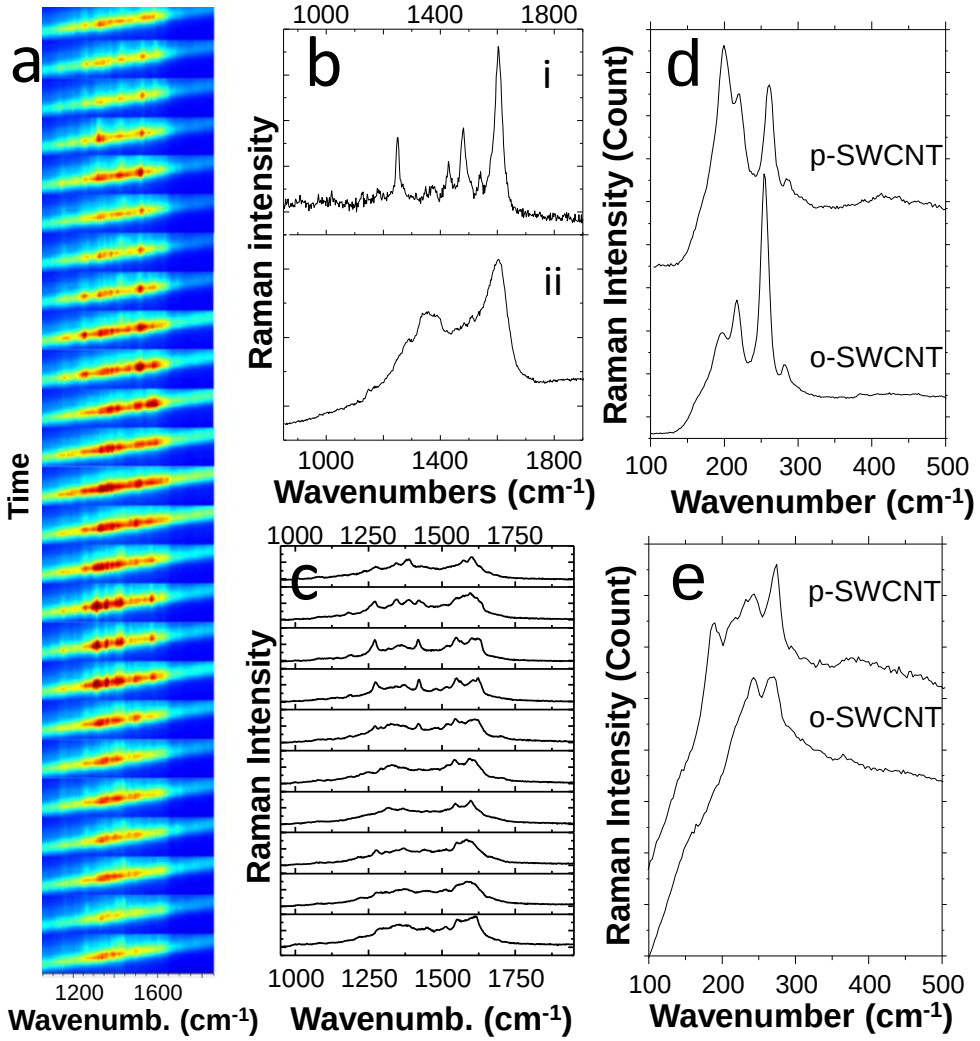

Fig 1. a) Intensity plots of consequently recorded temporally fluctuating SERRS spectra of p-SWCNTs ($\lambda_{excitation}$ = 532 nm). Each SERRS spectrum was acquired for 1s with a time interval of 10s. b) SERRS spectra acquired at different regions of the sample ($\lambda_{excitation}$ = 532 nm): i) a region where no temporal fluctuations occur and ii) a region of the sample showing variation in the spectral profile over time. c) Ten spectra taken from the series in a), the band intensities have been normalised for clarity and a background correction has been performed. d) SERRS spectra in the RBM spectral region. $\lambda_{excitation}$ = 632 nm, e) SERRS spectra in the RBM spectral region. $\lambda_{excitation}$ = 532 nm.

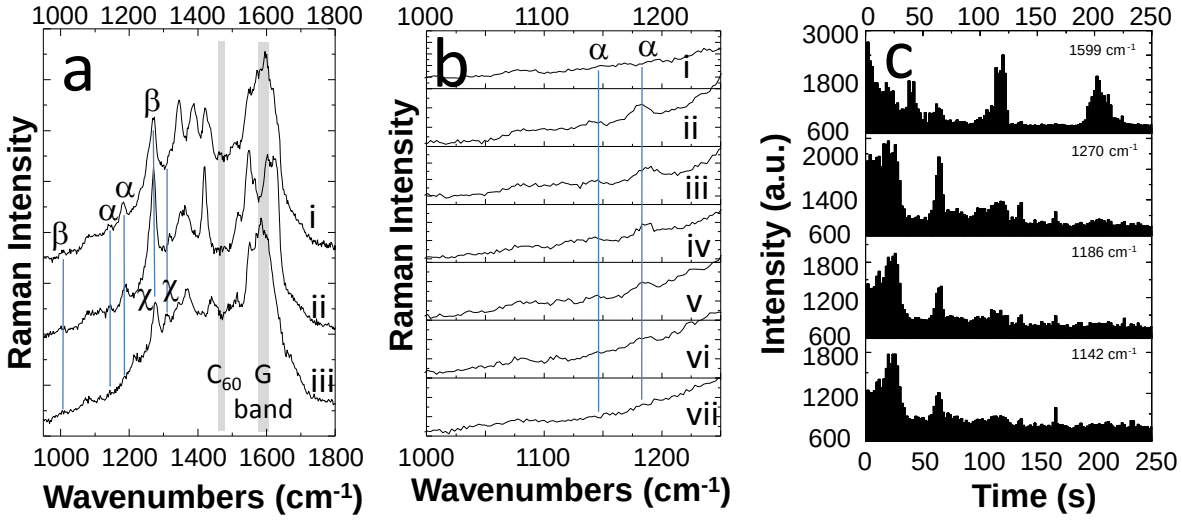

Fig 2. Temporally fluctuating SERRS spectra of p-SWCNTs. $\lambda_{excitation}$ = 532 nm. Each SERRS spectrum was acquired with a time interval of 10s. a) three spectra taken from Fig 1c, α , β and χ mark band positions. b) magnified sections of the spectra shown in Fig 1d, the band intensities have been normalised for clarity. c) a plot of peak intensity vs time for temporally fluctuating SERRS peak intensities acquired with a time interval of 2s as a function of time over 250 s.

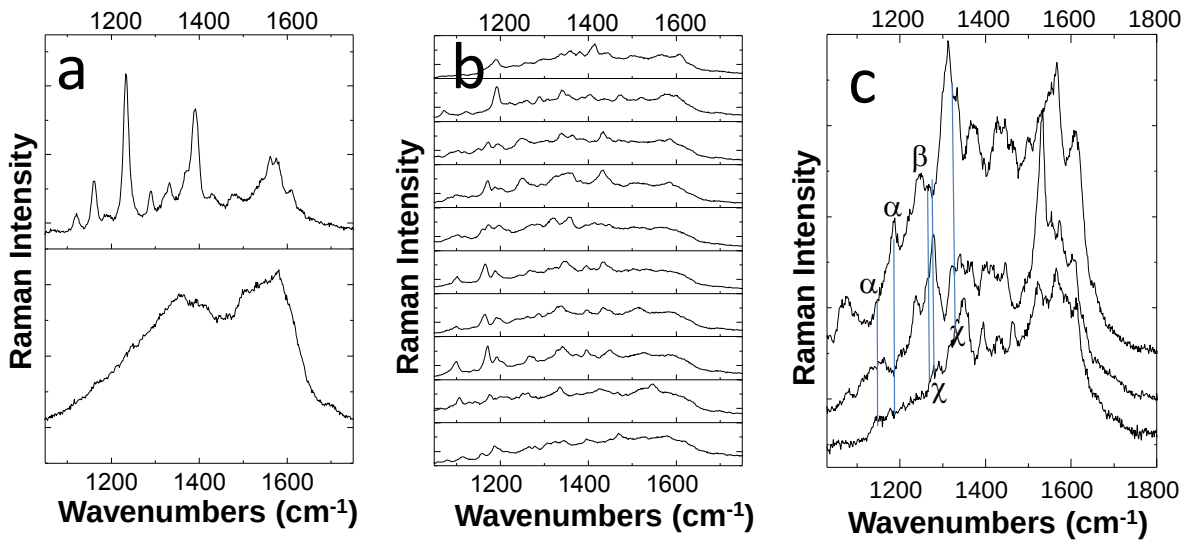

Fig 3. Temporally fluctuating SERRS spectra of p-SWCNTs. $\lambda_{excitation}$ = 632 nm Each SERRS spectrum was acquired with a time interval of 10s. The spectra are normalized for clarity. a) Two spectra taken from different parts of the sample. b) a series of ten spectra taken consecutively. c) Three spectra from Fig 3a enlarged for clarity.

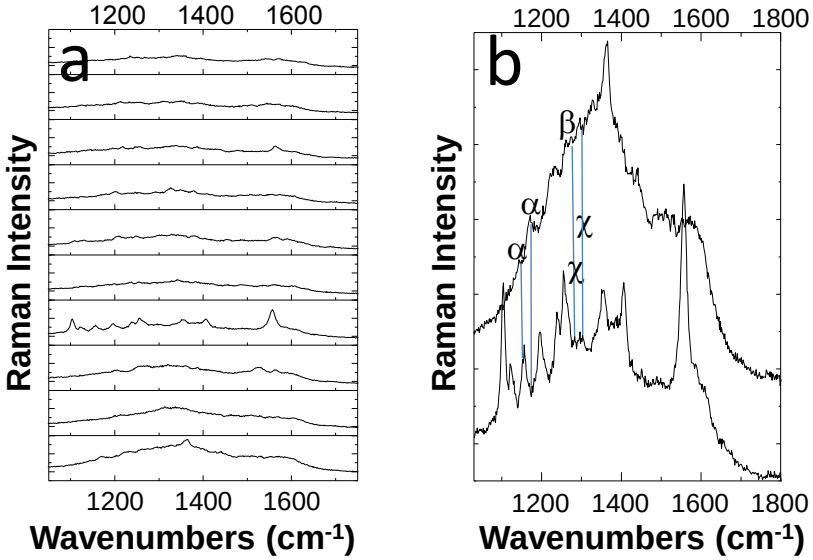

Fig 4. a) Temporally fluctuating SERRS spectra of o-SWCNTs. $\lambda_{excitation}$ = 632 nm Each SERRS spectrum was acquired with a time interval of 10s. The spectra are normalized for clarity. b) Two spectra from Fig 3a enlarged.

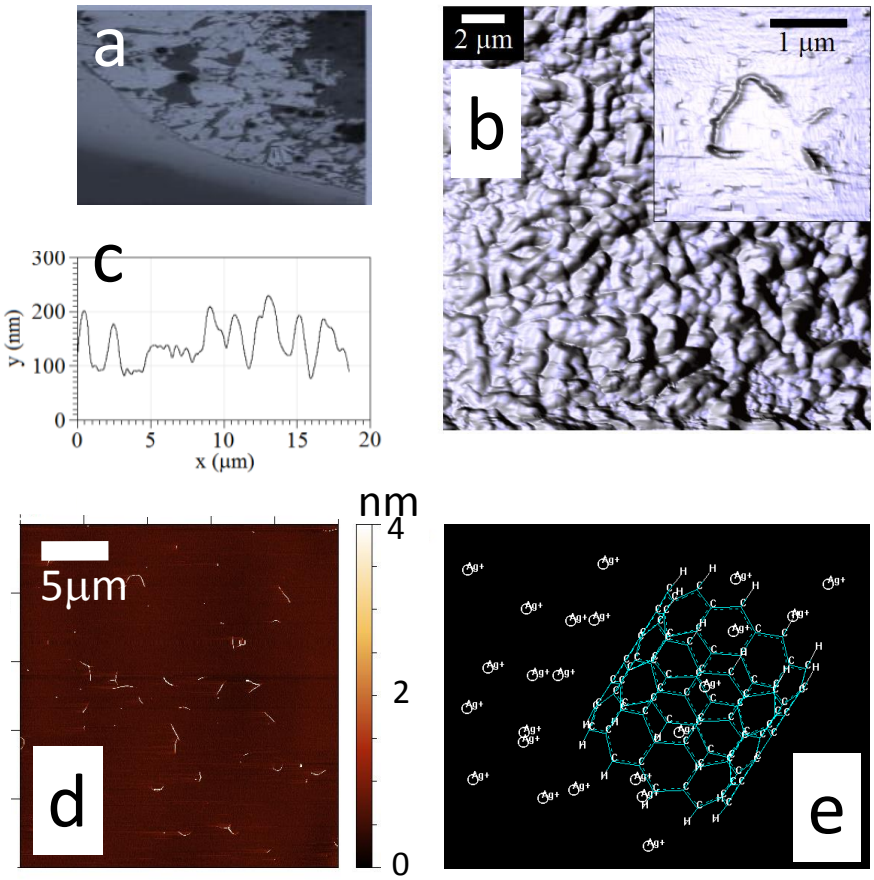

Fig. 5 a) optical microscope image of a SERRS substrate. b) AFM topography image of the substrate surface. inset shows SWCNTs bundles on the silver surface recorded on a relatively smooth part of the surface. c) shows a AFM topography profile plot showing a roughness on the order of 10s to 100 nm. d) AFM topography image of o-SWCNTs deposited onto a glass slide. e) Molecular dynamics simulation of the interaction of silver ions and a nanotube structure.